Measuring *Caenorhabditis elegans* Spatial Foraging and Food Intake Using Bioluminescent Bacteria

Siyu Serena Ding,*,† Maksym Romenskyy,‡ Karen S. Sarkisyan,*,† and Andre E. X. Brown*,†,1

*Institute of Clinical Sciences, Imperial College London, London W12 0NN, United Kingdom, ‡Department of Life Sciences, Imperial College London, London SW7 2AZ, United Kingdom, and †Medical Research Council London Institute of Medical Sciences, London W12 0NN, United Kingdom

ORCID IDs: 0000-0002-8590-3908 (S.S.D.); 0000-0003-2565-4994 (M.R.); 0000-0002-5375-6341 (K.S.S.); 0000-0002-1324-8764 (A.E.X.B.)

ABSTRACT For most animals, feeding includes two behaviors: foraging to find a food patch and food intake once a patch is found. The nematode *Caenorhabditis elegans* is a useful model for studying the genetics of both behaviors. However, most methods of measuring feeding in worms quantify either foraging behavior or food intake, but not both. Imaging the depletion of fluorescently labeled bacteria provides information on both the distribution and amount of consumption, but even after patch exhaustion a prominent background signal remains, which complicates quantification. Here, we used a bioluminescent *Escherichia coli* strain to quantify *C. elegans* feeding. With light emission tightly coupled to active metabolism, only living bacteria are capable of bioluminescence, so the signal is lost upon ingestion. We quantified the loss of bioluminescence using N2 reference worms and *eat-2* mutants, and found a nearly 100-fold increase in signal-to-background ratio and lower background compared to loss of fluorescence. We also quantified feeding using aggregating *npr-1* mutant worms. We found that groups of *npr-1* mutants first clear bacteria from within the cluster before foraging collectively for more food; similarly, during large population swarming, only worms at the migrating front are in contact with bacteria. These results demonstrate the usefulness of bioluminescent bacteria for quantifying feeding and generating insights into the spatial pattern of food consumption.

KEYWORDS bioluminescence; imaging; *Caenorhabditis elegans*; foraging; food distribution; feeding rate

FEEDING behavior plays an important role in fields ranging from ecology and evolution (MacArthur and Pianka 1966; Larsen 2003) to ageing and metabolism (Trepanowski *et al.* 2011; Balasubramanian *et al.* 2017) and health and disease (Mattson *et al.* 2014; Djalalinia *et al.* 2015). The roundworm *Caenorhabditis elegans* has emerged as a useful model organism to study all aspects of feeding, including the immediate response to finding food (Sawin *et al.* 2000), foraging, and patch leaving (Shtonda 2006; Harvey 2009; Bendesky *et al.* 2011; Milward *et al.* 2011; Scott *et al.* 2017b), as well as the details of food intake (Avery 1993; Avery and Shtonda 2003; Fang-Yen *et al.* 2009) and even spitting (Bhatla *et al.* 2015).

doi: https://doi.org/10.1534/genetics.119.302804
Manuscript received September 5, 2019; accepted for publication January 6, 2020; published Early Online January 7, 2020.
Supplemental material available at figshare: https://doi.org/10.25386/genetics.11535675.
[1]Corresponding author: Institute of Clinical Sciences, Imperial College London, Du Cane Rd., London W12 0NN, UK. E-mail: andre.brown@imperial.ac.uk

These studies of the genes and neural circuits underlying feeding rely on a variety of methods that have been developed to quantify feeding in *C. elegans*. *C. elegans* feeds by sucking bacteria into its mouth using rhythmic pumping of its pharynx (Avery and You 2012), and pharyngeal pumping frequency is often used as a proxy for food intake. Because worms are transparent, pharyngeal pumping can be measured manually by direct observation under a stereomicroscope or, more recently, using automated image analysis (Scholz *et al.* 2016). Electrophysiological readouts can also be used to measure multiple worms in parallel in microfluidic devices (Lockery *et al.* 2012). Alternatively, feeding can be measured using a nonfood additive such as exogeneous luciferin (Rodríguez-Palero *et al.* 2018), dye (You *et al.* 2008), or fluorescent beads (Fang-Yen *et al.* 2009; Kiyama *et al.* 2012). Bacteria consumption can also be measured directly by optical density in liquid (Gomez-Amaro *et al.* 2015) or by using fluorescently labeled bacteria. Labeled bacteria can provide a quantitative measurement of food inside the worm gut using a worm sorter (Andersen *et al.* 2014) or

image analysis (You *et al.* 2008), and consumption can be measured on solid media using a plate reader (Zhao *et al.* 2018).

How food is distributed and consumed in space crucially affects the animal's foraging strategy (Bernstein 1975; Stenberg and Persson 2005; Lanan 2014; Ding *et al.* 2019b) and subsequent fitness. Therefore, of the existing methods of quantifying feeding, imaging the consumption of fluorescently labeled bacteria is of particular interest since it can provide information on both where and how much food has been consumed (Gloria-Soria and Azevedo 2008). However, as fluorescent proteins form stable cooperatively folding structures, they are resistant to proteolytic cleavage (Bokman and Ward 1981; Nicholls and Hardy 2013). This results in high background fluorescence signal even after bacteria are digested by *C. elegans*, complicating both the quantification and the interpretation of feeding behavior.

Here, we use an *Escherichia coli* strain with self-sustained bioluminescence to monitor both the rate of food intake and its spatial distribution in laboratory reference and mutant worms, worms treated with serotonin and naloxone, and in large population worm swarms.

Materials and Methods

C. elegans maintenance and synchronization

C. elegans strains used in this study are listed in Table 1. All worms were grown on *E. coli* OP50 at 20° as mixed-stage cultures under uncrowded and unstarved conditions, and maintained as described (Brenner 1974). Synchronized young adult animals were used for all imaging experiments, and they were obtained by bleach-synchronization and subsequent refeeding of starved L1s on OP50 for 65–72 hr at 20°.

Measuring 40-worm feeding with bioluminescent or fluorescent bacteria

A step-by-step protocol can be found at: dx.doi.org/10.17504/protocols.io.5hsg36e.

For every set of experiments, a fresh overnight liquid culture of DH5α-ilux or OP50-GFP was grown by inoculating a single bacterial colony into 100 ml of LB broth containing 50 μg/ml ampicillin, and incubating for 16–18 hr at 37° at 220 rpm. The liquid culture was allowed to cool down to room temperature for 3–6 hr before use. Then, 20 μl of the liquid culture was seeded onto the center of a 35 mm low-peptone (0.013% w/v) NGM plate and dried in a laminar flow hood (Heraguard) for 0.5 hr. Synchronized young adult worms were harvested and washed in M9 buffer, and 40 animals were transferred onto the seeded plate using a glass pipette without disturbing the bacterial lawn. After M9 was absorbed into the media, the imaging plate was gently vortexed for 10 sec on the lowest setting of a vortex mixer (Vortex-Genie 2; Scientific Industries) to randomize initial worm positions. Imaging acquisition commenced 1 min after the vortex start.

Imaging was performed using the IVIS Spectrum imaging system (Caliper LifeSciences) and Living Image software (v4.3.1) for all experiments except those in Supplemental Material, Figure S4. For bioluminescence, 1 sec exposures were used with blocked excitation and open emission filters; for fluorescence, 0.5 sec exposures were used with 465 nm excitation and 520 nm emission filters. Images were acquired every 6 min for up to 13.5 hr at 20°. Field-of-view option C (13.5 cm × 13.5 cm) was used to allow simultaneous imaging of up to nine 35 mm plate-feeding samples in 3 × 3 configuration, where at least one sample is a no-worm control to enable subsequent signal normalization.

For experiments in Figure S4, imaging was performed using the commercial-grade α7 III digital camera (Sony, Tokyo, Japan) with the FE 90 mm F2.8 Macro G OSS lens (Sony). The camera was mounted on a tripod to image from above the samples. ISO 16,000, F2.8, and 30 sec exposure were used to image bioluminescence. Images were acquired every 6 min for up to 12 hr at 22° inside a dark room. A no-worm control was included with every experiment to enable subsequent signal normalization.

Measuring feeding during large population swarming with bioluminescent or fluorescent bacteria

A step-by-step protocol can be found at: dx.doi.org/10.17504/protocols.io.53kg8kw.

The bacteria overnight liquid culture was grown as described above. Briefly, 500 μl of the liquid culture was seeded onto the center of a 90 mm low-peptone (0.013% w/v) NGM plate and dried in a laminar flow hood (Heraguard) for 2.5 hr. A separate 20 μl liquid culture was seeded onto the center of a 35 mm low-peptone plate and dried in a laminar flow hood (Heraguard) for 0.5 hr to serve as a no-worm control. Synchronized young adult worms were harvested and washed in M9 buffer, and a few thousand animals were transferred onto the seeded 90 mm plate using a glass pipette without disturbing the bacterial lawn.

Imaging acquisition commenced immediately after worm transfer using the IVIS Spectrum imaging system (Caliper LifeSciences) and Living Image software (v4.3.1). For bioluminescence, 1 sec exposures were used with blocked excitation and open emission filters; for fluorescence, 1 sec exposures were used with 465 nm excitation and 520 nm emission filters. Images were acquired every 2 min for up to 4.5 hr at 20°. Field-of-view option C (13.5 cm × 13.5 cm) was used to allow simultaneous imaging of one 90 mm plate swarming sample and one 35 mm plate no-worm control, the latter of which was used for subsequent signal normalization.

Measuring 40-worm feeding after drug treatments

A step-by-step protocol can be found at: dx.doi.org/10.17504/protocols.io.53ng8me.

The protocol is essentially the same as the 40-worm feeding measurement protocol above, except for two differences: (1) imaging plates are now low-peptone NGM plates also

containing drugs (20 mM serotonin or 10 mM naloxone), and (2) young adult N2 worms were prestarved on an unseeded NGM plate for 1 hr before being transferred onto seeded drug plates, and imaging commenced following a 1-hr drug exposure instead of immediately following worm transfer.

Drug plates were freshly prepared the day before each experiment. For serotonin (H7752; Sigma-Aldrich, St. Louis, MO) treatment, low-peptone NGM agar was prepared and serotonin was added to molten agar to a final concentration of 20 mM before the agar was dispensed into 35 mm plates. For naloxone (PHR1802; Sigma-Aldrich), a 10x stock solution was freshly prepared in water and 300 μl was spread on top of a 35 mm plate containing 3 ml low-peptone NGM agar to achieve a final concentration of 10 mM. The naloxone plates were dried in a laminar flow hood (Heraguard) for 3 hr before all drug plates were wrapped in foil and stored at 4° overnight for immediate use the next day.

To track worm positions following drug treatments, bright-field imaging was performed using a custom-built six-camera rig equipped with Dalsa Genie cameras (G2-GM10-T2041) rather than the IVIS Spectrum imaging system. One-hour recordings were performed with 630 nm LED illumination (CCS Inc.) at 25 Hz using Gecko software (v2.0.3.1), and worm positions were extracted from the pixel data using a MATLAB (R2018b) script.

Measure pharyngeal pumping after drug treatments

Drug plates were prepared as described above, and were used either unseeded or seeded with 20 μl of DH5α-ilux overnight liquid culture. Prestarved N2 young adult worms were transferred to drug plates with or without food as described above, and were exposed to the drugs for 1 hr before pharyngeal pumping was assessed. The number of pumps was scored over 60 sec under a stereomicroscope (Stemi 508; Zeiss, Oberkochen, Germany).

Signal processing for feeding experiments

For imaging data acquired on the IVIS Spectrum, bioluminescence or fluorescence raw signals (photons/sec) were extracted from user-defined regions of interest (ROI) using Living Image software (v4.3.1). Each ROI corresponds to the full area of the circular image plate (35 mm or 90 mm radius).

For imaging data acquired using the Sony camera, signal from a dark image was first subtracted from a raw image before the red channel was dropped from the analysis. The RGB image was then converted to grayscale and a median filter was applied. Finally, signals from ROI were extracted using a MATLAB (R2018b) script for downstream analysis.

Feeding rate analysis

For each feeding experiment, the signal time series was divided by the level detected in the first frame. This relative signal was further normalized to the value of the corresponding no-worm control at each time point to correct for the nonstationarity of the signal in the absence of feeding. Relative feeding rates were then estimated by taking the derivative of the normalized signals over time.

Roughness calculation for large population swarming experiments

To detect the moving front in each swarming experiment, the ROI was first defined based on the outline of the intact food patch automatically detected from the bioluminescence channel. The ROI was subsequently overlaid on the bright-field video and only frames containing an unbroken moving front of the swarm within the ROI (Supplemental Movies 5 and 6) were chosen for further processing. Next, each bright-field frame was segmented through stepwise thresholding and the boundary of the moving front was detected. This boundary was segmented further to extract only the pixels corresponding to the leading edge of the swarm (Supplemental Movies 5 and 6). The resulting curve (green in Figure 4D) was then fitted with a best-fit circle using the Pratt method (Pratt 1987). Finally, the roughness of the leading edge W was computed as the variance of the radial distance between the leading edge and the center of the best-fit circle:

$$W(t) = \sqrt{[h(t) - \bar{h}(t)]^2},$$

where t denotes time (*i.e.*, a movie frame), h is the distance from a point on the leading edge to the center of the best-fit circle, and $\bar{h}$ stands for the spatial average over the whole leading edge of the migrating front. This analysis was performed using a MATLAB (R2019b) script.

Data availability

Strains are available upon request. The authors affirm that all data necessary for confirming the conclusions of the article are present within the article and figures. Supplemental material available at figshare: https://doi.org/10.25386/genetics.11535675.

Results

Bioluminescent bacteria improve signal-to-background ratio in a feeding assay

Previous studies have used fluorescent protein-expressing strains of *E. coli* to measure worm feeding. However, when we recorded worms feeding on *E. coli* strain OP50-DsRed, we noticed a prominent background fluorescence signal, which was especially conspicuous in our experiments with DA609 (*npr-1* aggregation mutant) worms (Figure 1A, red arrow). These worms first form aggregates on food and then collectively swarm over the food patch, which leads to local food depletion (Ding *et al.* 2019a). It is possible that a fraction of DsRed molecules survives passage through the worm gut due to resistance to protease cleavage. Background signal may also result from fluorescent protein molecules that seeped into the medium from the cytoplasm of dead bacterial cells or have been expelled with liquid as a normal part of pharyngeal pumping. Alternatively, the background may be attributable to a small number of bacteria at a density that is low enough for worms to ignore, although this seems unlikely given that the background "halo" can be quite bright (Figure 1A, red arrow). These three possible sources of fluorescence

Table 1 Materials and reagents used in this study

Resource	Designation	Source or reference	Identifier	Additional information
Strain (*C. elegans*)	N2	*Caenorhabditis* Genetics Centre	RRID:WB-STRAIN:N2	Laboratory reference strain
Strain (*C. elegans*)	DA1116	*Caenorhabditis* Genetics Centre	RRID:WB-STRAIN:DA1116	Genotype: *eat-2(ad1116)II*.
Strain (*C. elegans*)	DA609	*Caenorhabditis* Genetics Centre	RRID:WB-STRAIN:DA609	Genotype: *npr-1(ad609)X*.
Strain (*E. coli*)	DH5α-ilux	Addgene	RRID:Addgene_107879	Contains ilux pGEX(-)
Strain (*E. coli*)	OP50-GFP	Jonathan Hodgkin (University of Oxford)	RRID:WB-STRAIN:OP50-GFP	
Strain (*E. coli*)	OP50-DsRed	Jonathan Hodgkin (University of Oxford)		
Equipment	IVIS Spectrum In Vivo Imaging System	PerkinElmer	124262	
Equipment	α7 III camera	Sony	ILCE-7M3	
Equipment	FE 90 mm F2.8 macro G OSS lens	Sony	SEL90M28G	
Equipment	Tripod	Manfrotto	MK055XPRO3-BHQ2	
Software, algorithm	Living Image software	PerkinElmer	RRID:SCR_014247	Version 4.3.1
Software	MATLAB	MathWorks		Version R2018b
Chemical compound, drug	Serotonin	Sigma-Aldrich	H7752	
Chemical compound, drug	Naloxone	Sigma-Aldrich	PHR1802	

background are not mutually exclusive and complicate the quantification and interpretation of feeding experiments. The background remained when we used a different fluorophore (*E. coli* OP50-GFP, Figure 1B, middle) or a different worm strain that does not aggregate (*C. elegans* N2, Figure 1B, right).

As an alternative to fluorescence-based bacterial labeling, we tested a bioluminescent *E. coli* strain (DH5α-ilux) as the worm food source. We transformed *E. coli* DH5α with the high copy-number ilux pGEX(−) plasmid containing an engineered *Photorhabdus luminescens lux* operon (ilux) (Gregor *et al.* 2018). This operon encodes enzymes of a bacterial bioluminescence system, where the enzymes perform biosynthesis, oxidation, and recycling of a long-chain fatty aldehyde, the key component of the light-emitting reaction along with flavin mononucleotide. The ilux operon is under the control of a leaky *tac* promoter (de Boer *et al.* 1983) that provides constitutive expression in *E. coli* throughout the experiment. Active bacterial metabolism is required for bioluminescence production from the ilux operon.

We seed a defined quantity of DH5α-ilux liquid culture onto NGM plates, let a population of 40 worms feed, and monitor food consumption over time using an IVIS Spectrum imaging system. We show that following DA609 or N2 feeding experiments that result in total food exhaustion, the bioluminescence imaging method gives very reduced background when normalized to the starting signal (Figure 1C), in contrast to fluorescence imaging, which shows noticeable background levels (Figure 1B). Feeding assays using bioluminescent bacteria shows a nearly 100-fold increase in signal-to-background ratio compared to using fluorescent bacteria (Figure 1, B and C).

Bioluminescence depends on growth conditions and provides a quantitative measurement of worm feeding rates

Since bioluminescence from DH5α-ilux depends on active bacterial metabolism, we next characterized signal strength under different experimental conditions. Storing bacterial culture at 4° overnight abolishes the signal, so a fresh overnight culture was prepared for all experiments. We grew DH5α-ilux in overnight liquid cultures at 37° to stationary phase and allowed them to cool down to room temperature before seeding onto NGM media for imaging. Serial dilution of the overnight liquid culture shows roughly linear scaling with bacteria concentration (Figure 2A, $R^2 = 0.976$). After seeding 20 μl of overnight culture onto NGM plates containing different levels of peptone (regular peptone, 0.25% w/v; low peptone, 0.013% w/v; no peptone, 0% w/v), bioluminescence signal was monitored for hours (Figure 2B) and days (Figure 2C) at 20°. As expected, the signal is the highest on media with the highest peptone concentration (Figure 2, B and C, blue lines) and lowest on no-peptone media (Figure 2, B and C, black lines). On standard NGM (0.25% w/v peptone), bioluminescence increases for ∼1 week and then decreases over several days, with no obvious stationary plateau (Figure 2C, blue line); On the scale of hours, there is an initial decrease in intensity over the first few hours followed by an ∼5-fold increase over the next day (Figure 2B, blue line). This initial decrease perhaps represents a lag phase of growth on solid media. All subsequent experiments were performed on low-peptone (0.013% w/v) NGM media. Taken together, bioluminescence signal strength from DH5α-ilux depends on a number of growth conditions that affect bacterial metabolism, including temperature, peptone level, and inoculation time.

We next compared the population feeding rates of the laboratory reference N2 strain and DA1116, an *eat-2* mutant with abnormal neurotransmission in the pharynx (McKay *et al.* 2004) that pumps slowly (Raizen *et al.* 1995). To take into account different initial bioluminescence levels across experimental samples (Figure 2D), we divide the signal in each condition by the level detected in the first frame. This relative signal is then further normalized to the value of the

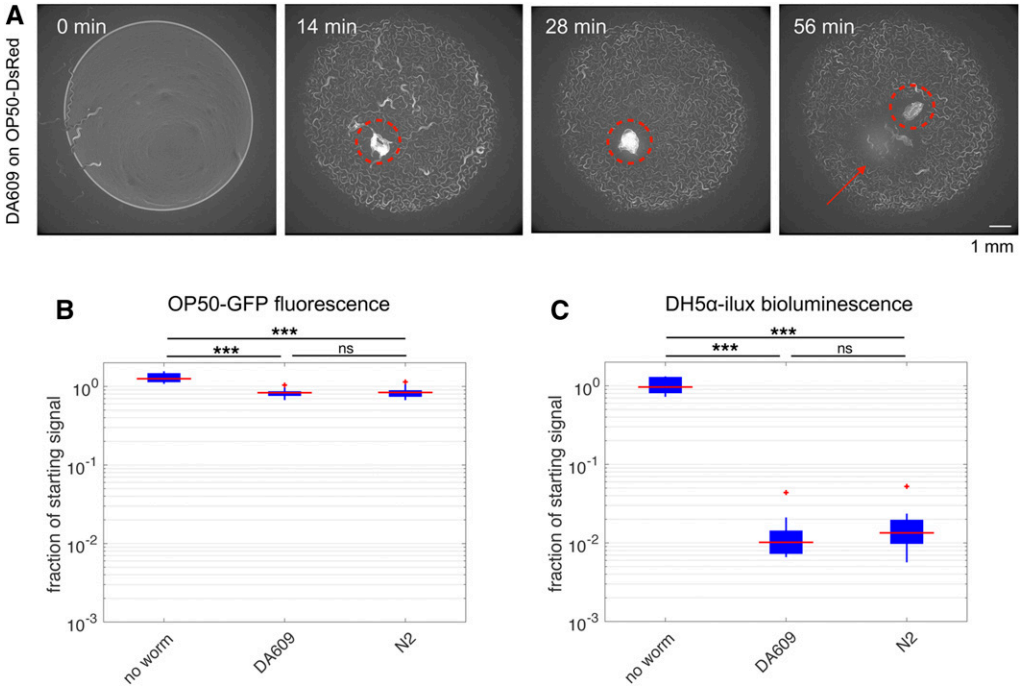

Figure 1 Assessing worm feeding behavior with bacteria labeling. (A) Sample snapshots of a group of 40 DA609 worms feeding on a fluorescent *E. coli* OP50-DsRed lawn. Red circles show the worm aggregate, and the red arrow points to the remaining background signal after the worm cluster moves away from its original site. (B and C) Background signal comparison between fluorescence (B) and bioluminescence (C) methods. Population feeding experiments were performed on low-peptone NGM plates seeded with fluorescent *E. coli* OP50-GFP (B) or bioluminescent *E. coli* DH5α-ilux (C). Zero ("no worm") or 40 ("DA609" and "N2") worms were allowed to feed on and deplete the bacteria for 13.5 hr. Signal from the labeled bacteria was obtained at the start (100% food) and at the end (0% food) of the experiment using the fluorescence (465 nm excitation, 520 nm emission) or the bioluminescence (no excitation, open emission) imaging protocol, and the final to starting signal ratios were calculated. For the boxplots in B and C, the red horizontal line indicates the median, the bottom and top edges of the box indicate the 25th and 75th percentiles, respectively, and the whiskers extend to the most extreme data points excluding the outliers, which are plotted individually using the red "+" symbol. For both B and C, $n = 5$ for no worm, $n = 10$ for DA609, and $n = 11$ for N2, pooled between four independent sets of experiments. *** $P < 0.01$; ns: $P > 0.05$, two-sample *t*-test of the replicate means.

corresponding no-worm control at each time point to correct for the nonstationarity of the signal in the absence of feeding (Figure 2E). Relative feeding rates are then estimated by taking the derivative of the normalized signals over time (Figure 2F). Since the normalization is important for reliable estimation of the feeding rate, we recommend including no-worm controls whenever possible.

We show that both N2 and DA1116 worm strains deplete the food at a roughly constant rate (Figure 2, E and F), and that the median feeding rate from the first 4 hr (before N2 runs out of food) for DA1116 is 41% that of N2. DA1116's reduced feeding rate on solid media is consistent with previous reports of its slow pumping (~10% that of N2; Raizen *et al.* 1995) and restricted food intake in liquid-based assays [~80% that of N2 as measured by optical density-based bacterial clearing (Gomez-Amaro *et al.* 2015) and ~60% that of N2 as measured by luciferin ingestion (Rodríguez-Palero *et al.* 2018)]. The variability in reported relative feeding rates may be due to different measurements and assay conditions (pumping motion *vs.* ingested particles, natural *vs.* artificial food, solid- *vs.* liquid-based assays). Our experiment also confirms that the signal from freshly inoculated overnight liquid culture is sufficient to estimate relative feeding rates. For less-sensitive imaging instruments, it would be possible to incubate seeded plates for longer to obtain higher signal (Figure 2C).

We repeated the feeding experiments and analysis using OP50-GFP bacteria (Figure S1) instead of DH5α-ilux, and obtained similar results showing that DA1116 feeding rate is 49% that of N2 despite a very different no-worm control signal (Figure S1A, black line). This highlights the importance of normalization using either bacteria labeling method. While the relative feeding rate results are reassuringly similar between bioluminescence- and fluorescence-based methods, the fluorescence method shows a lower signal-to-background ratio as well as high background levels (Figure S1A) that may complicate analysis and interpretation when normalized (Figure S1, B and C).

Serotonin has previously been reported to enhance pharyngeal pumping and food intake (Horvitz *et al.* 1982; Niacaris and Avery 2003) as well as the slowing response of starved worms (Sawin *et al.* 2000). We thus prestarved N2 worms before exposing them to serotonin in the presence of food. Unexpectedly, serotonin treatment caused a decrease in the measured feeding rate (Figure S2A, blue and black lines). We observed a comparable reduction in feeding rate using OP50-GFP bacteria as the food source (Figure S2B, blue and black lines). We confirmed serotonin was having the expected effects on pumping rate (Figure S2D). However, in serotonin-treated samples, a smaller number of worms reaches the bacterial lawn (Figure S2, E and F), most likely due to serotonin's suppression of locomotion (Horvitz *et al.* 1982). Therefore, these results do not contradict previous findings but highlight the multifaceted effects of serotonin and the essential role of foraging in successful feeding.

In contrast to serotonin, the morphine antagonist naloxone has been reported to decrease food intake in starved worms by

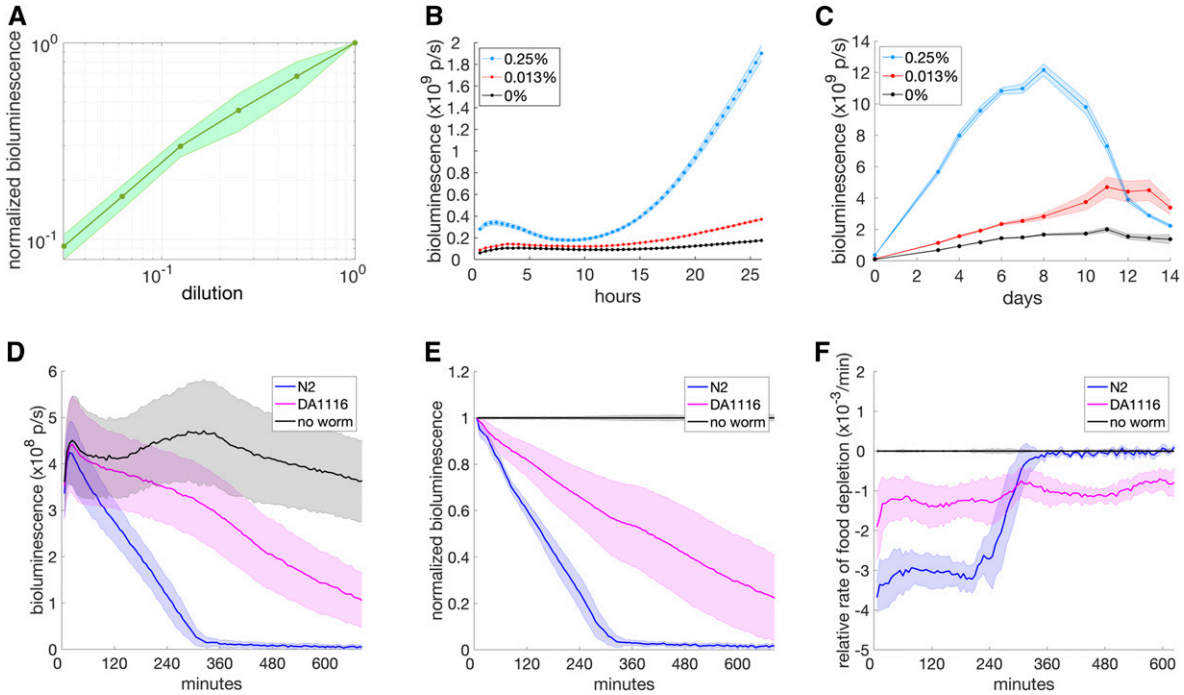

Figure 2 DH5α-ilux bioluminescence signal characterization. (A) Normalized signal from liquid bacteria culture in a twofold dilution series. Concentration of one is undiluted bacteria overnight culture. Signal is taken immediately following serial dilution in LB broth where all samples have a final volume of 150 μl, and are normalized to undiluted levels. Here $n = 9$, pooled between three independent sets of experiments. Error bars represent ± 1 SD. Linear regression of the data gives $R^2 = 0.976$. (B and C) Signal from 20 μl of bacteria culture after hours (B) and days (C) of incubation on solid NGM media containing different peptone levels. All incubations were performed at 20°, and all measurements were made following a 1 sec exposure. For B, signal was taken every 30 min and all samples were imaged simultaneously. $n = 3$ for each condition, error bars represent ± 1 SD. For C, signal was taken once on most days, $n = 3$, error bars represent ± 1 SD. (D–F) Bioluminescence from population feeding experiments of N2 and DA1116 worms, showing (D) raw signal, (E) normalized signal (normalized to the starting signal and then to the control signal), and (F) derivative of the normalized signal calculated over a 60-min window). Forty N2 (blue) worms, 40 DA1116 (magenta) worms, or no-worm control (black) experiments were performed on a 20 μl DH5α-ilux lawn. Measurements were taken every 6 min using 1 sec exposure. All samples shown were imaged simultaneously. Here $n = 11$ for N2, $n = 10$ for DA1116, and $n = 5$ for control, pooled from four independent sets of experiments; error bars represent ± 1 SD. p/s, photons/sec.

acting on an opioid receptor expressed in a sensory neuron (Cheong *et al.* 2015). Naloxone treatment did result in a decreased feeding rate as expected (Figure S2A, red and black lines), but the levels of bioluminescence were much lower than in naloxone-free controls (Figure S2C, left). We again confirmed that the feeding rate was reduced using OP50-GFP bacteria (Figure S2B, red and black lines). Fluorescence levels were decreased compared to controls (Figure S2C, right), but the effect was not drastic and naloxone does not detectably affect *E. coli* growth (Maier *et al.* 2018), suggesting that naloxone may act more specifically on bioluminescence-related metabolism.

Bioluminescent bacteria reveal the spatial aspect of C. elegans feeding behavior

To gain insights into different *C. elegans* feeding strategies, we performed experiments with the laboratory reference strain N2 and DA609, an *npr-1* loss-of-function mutant. The former are solitary feeders whereas the latter are social, initially forming worm aggregates on food and then collectively swarming over the food patch due to local food depletion (Ding *et al.* 2019a). Our feeding experiments on DH5α-ilux bioluminescent bacteria show that DA609 and N2 populations both have stable feeding rates over time, and that DA609 has a feeding rate that is 62% that of N2 (Figure 3, A and B). Experiments with OP50-GFP fluorescent bacteria show a similar relative feeding rate of 57% (Figure S3). Thus the social feeders have a lower feeding rate than the solitary ones despite similar pharyngeal pumping rates (Choi *et al.* 2013), consistent with a previous report measuring the amount of fluorescently labeled bacteria inside worm guts (Andersen *et al.* 2014).

Bioluminescence imaging also provides spatial information and we examined the pattern of food depletion between the two feeding strategies and noted major differences. While N2 worms show gradual depletion of the whole food patch roughly uniformly (Figure 3C, top row; Supplemental Movie 1, middle row), DA609 worms deplete food in a highly localized manner starting at one point and sweeping over the surface (Figure 3C, bottom row; Supplemental Movie 1, top row). These foraging behaviors observed here by bacterial depletion are consistent with our previous results in which worms were imaged directly (Ding *et al.* 2019a).

Moreover, we noticed that when DA609 worms initially aggregate they are covered in bacteria (Figure 3, C and D,

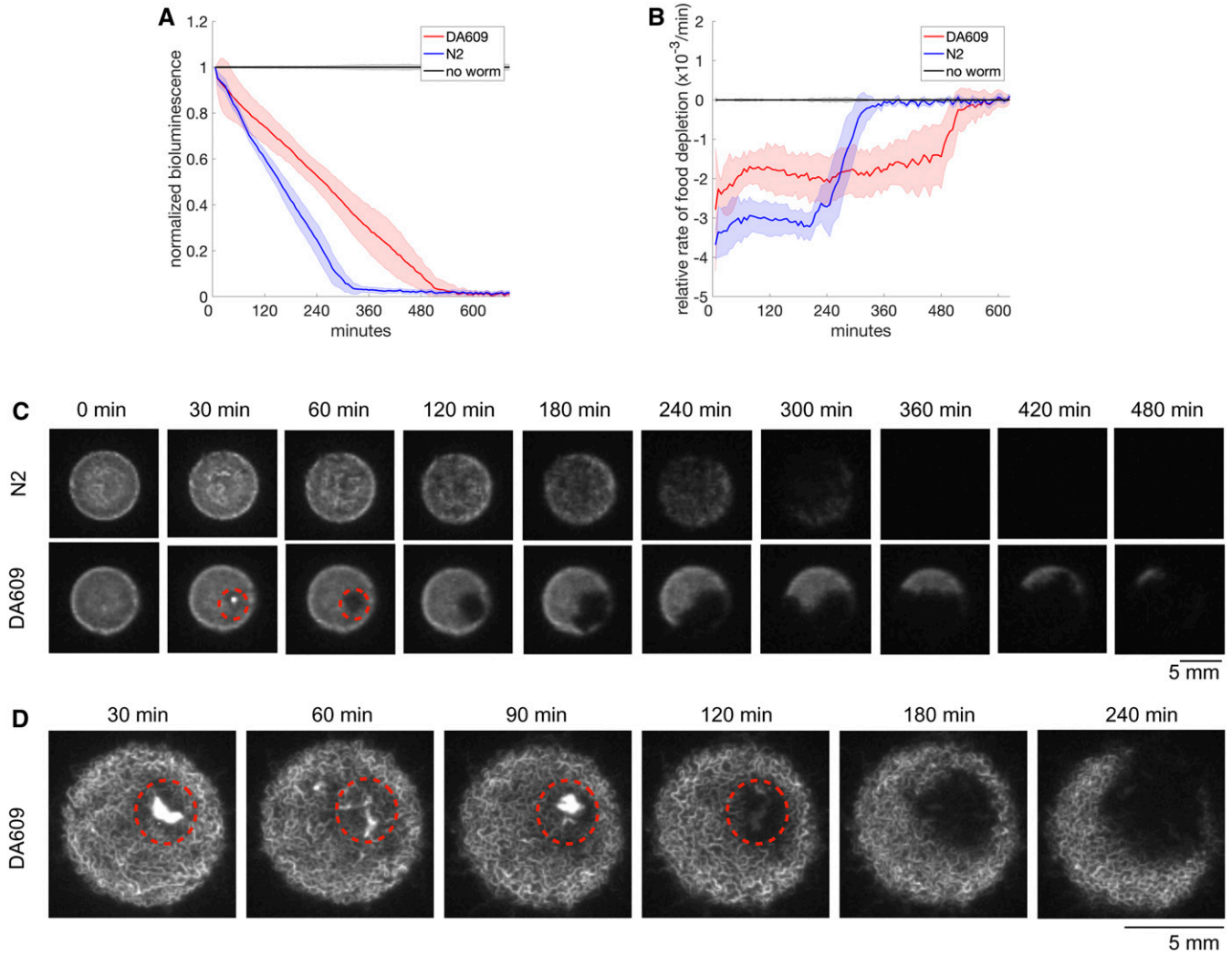

Figure 3 Bioluminescence from population feeding experiments of N2 and DA609 worms. (A) Normalized signal and (B) derivative of the normalized signal calculated over a 60-min window. Forty DA609 (red) or N2 (blue) worms or no-worm control (black) experiments were performed on a 20 μl DH5α-ilux lawn. We read 1 sec exposure measurements every 6 min; n = 11 for N2, n = 10 for DA609, and n = 5 for control, pooled from four independent sets of experiments; error bars represent ± 1 SD. (C) A series of snapshots contrasting the spatial pattern of food depletion in N2 (top) and DA609 (bottom) population feeding experiments. (D) A series of snapshots showing a DA609 worm aggregate (red circles) depleting food within the cluster first before moving onto new food.

30 min panels) and that the cluster stays in roughly the same place (Figure 3, C and D, red circles) until the in-cluster bacteria are completely consumed. This observation fits well with the distinct "aggregation" *vs.* "swarming" phases that we previously reported for DA609 (*npr-1*) aggregation (Ding *et al.* 2019a), suggesting that minimal cluster movement during the "aggregation" phase is due to the initial food availability inside the cluster. By contrast, the total depletion of bacteria inside the aggregate before collective movement starts is difficult to detect from the recordings of worms feeding on fluorescent bacteria, because the moving worm cluster is still fluorescent (Figure 1A, last panel; note the aggregation timescale is different for this experiment because OP50-DsRed bacteria were diluted). As mentioned previously, the source of this signal is unknown, but the bioluminescence results suggest that it is not due to residual metabolically active bacteria that adhere to the worm surface.

Finally, we have verified that the assay can also be performed using a commercial-grade digital SLR camera (Sony α7 III) that is compact, portable, and easy to use (see *Materials and Methods* for details). The imaging quality was sufficient to visualize contrasting spatial depletion patterns between the two worm strains (Figure S4A), and we found a relative feeding rate of 65% between DA609 and N2 (Figure S4, B and C), similar to the results we obtained with a cooled CCD camera (Figure 3).

Large-scale C. elegans swarms form a stable moving front on food

To study the behavior of larger populations of swarming worms, we imaged thousands of young adult N2 worms

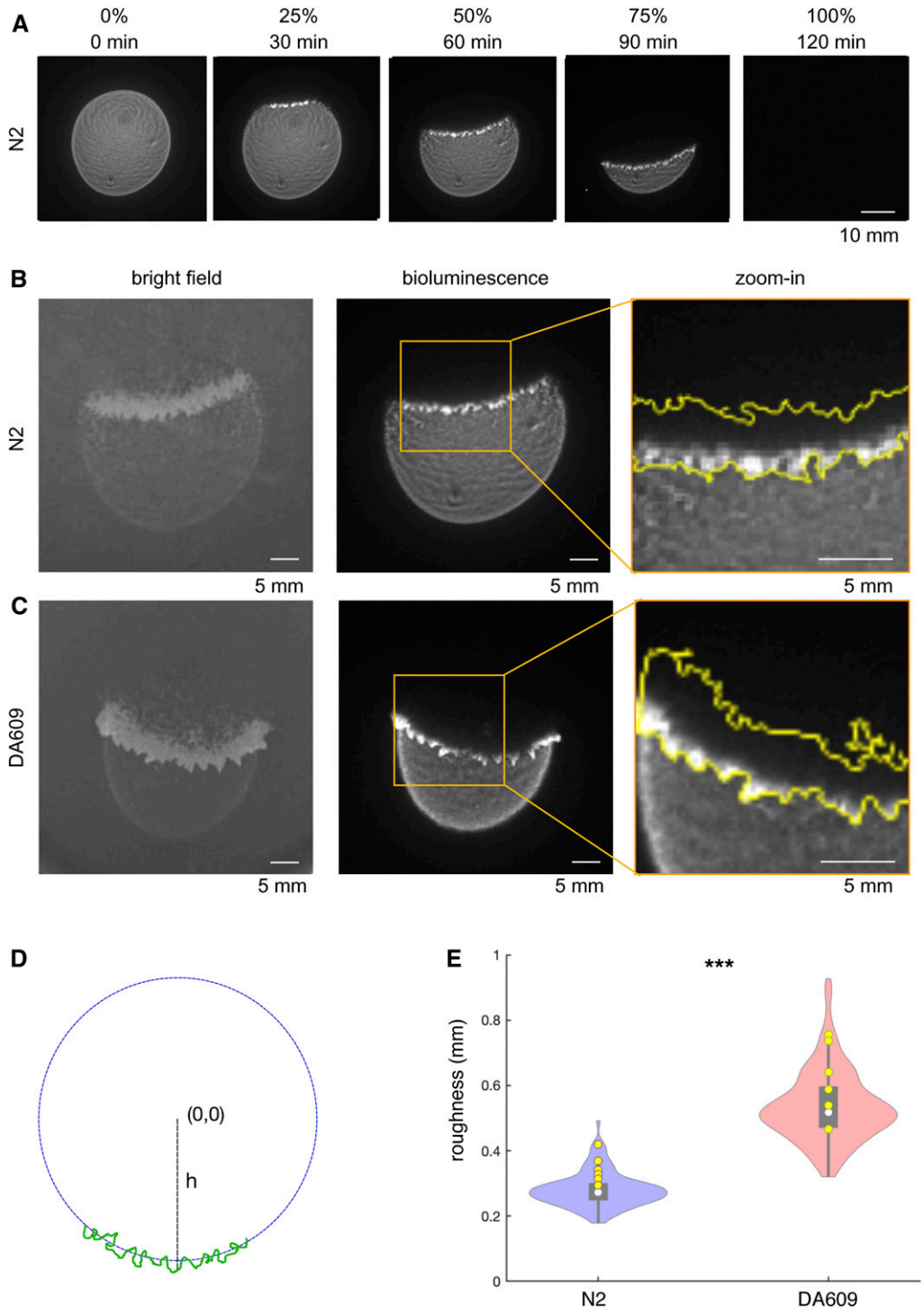

Figure 4 Bioluminescence signal from large population swarming experiments. A few thousand age-synchronized worms were allowed to feed and swarm over a 500 μl DH5α-ilux lawn. (A) Snapshots of a representative N2 swarming experiment on a DH5α-ilux lawn, with time progression to total food depletion indicated at the top. (B and C) Sample snapshots from N2 (B) and DA609 (C) swarming experiments, showing bright-field (left) and bioluminescence (middle) channels. The boxes in the middle panels are zoomed in and displayed on the right. The worm front outlines (yellow lines, right) were automatically extracted from the bright-field channel and overlaid onto bioluminescence images (Supplemental Movies 5 and 6). (D) Schematic drawing of roughness calculations (see *Materials and Methods* for details). After the segmentation steps, the resulting curvy front (green) was fitted with a best-fit circle. The roughness of the leading edge was computed as the variance of the radial distance (h) between points on the leading edge and the center (0,0) of the best-fit circle. (E) Roughness for N2 and DA609 swarming experiments. Yellow circles show mean roughness from each of the six replicates per strain. Violin plots show the distribution of frames sampled from all experimental replicates per strain: on each plot, the white circle indicates the median, the bottom and top edges of the box indicate the 25th and 75th percentiles, respectively, and the whiskers reach up to 1.5 times the interquartile range. The violin plot outlines illustrate kernel probability density, *i.e.*, the width of the shaded area represents the proportion of the data located there. *** P = 0.0013, Kolmogorov–Smirnov test of the replicate means between the two strains (n = 6 per strain, from 12 independent experiments).

feeding on larger 500 μl patches of DH5α-ilux bacteria and observed coherent swarming as the migrating worm front consumes the bacterial lawn in a single pass (Figure 4A, Supplemental Movie 2). Similar results were seen using OP50-GFP, although the fluorescent background remains after the front has passed (Figure S5A, Supplemental Movie 3). Bacterial signal during swarming can be quantified using the same analysis methods as in 40-worm feeding experiments (Figure S6).

Large populations of DA609 worms also swarm (Figure 4C, Supplemental Movie 4). By overlaying the bioluminescence channel (Figure 4, B and C, middle) with the bright-field

images (Figure 4, B and C, left), it is clear that only worms at the leading edge of the migrating front are in contact with bacteria regardless of the worm strain (Figure 4, B and C, right). We confirmed these results using OP50-GFP bacteria (Figure S5, B and C), although the bacterial gradient is less obvious due to background fluorescence. Our results are similar to those in a recent study reporting a bacterial gradient in swarming *C. elegans* using OP50-GFP (Demir *et al.* 2019). Finally, DA609 swarms form pronounced finger-like projections at the leading edge of the migrating front that protrude into the bacterial lawn (Figure 4C; Figure S5C). The fingers are dynamic structures that change shape over time as the wave migrates (Supplemental Movie 4). Fingering is less obvious in N2 worms, confirmed by the lower roughness of the leading edge of the swarm compared with DA609 swarms (Figure 4, D and E).

Discussion

We have developed *C. elegans* feeding assays using bioluminescence-labeled bacteria. This method allows simultaneous quantification of food intake and visualization of food distribution, which are both important aspects of *C. elegans* feeding behavior even though food intake has previously received greater attention. We show that a bioluminescence-based method results in higher signal-to-background ratios that simplify analysis and interpretation compared to fluorescence-based methods. Compared with other imaging-based methods, our method directly measures the ingestion of bacteria, rather than estimating bacterial uptake using exogeneous dye (You *et al.* 2008), beads (Fang-Yen *et al.* 2009), or luciferin (Rodríguez-Palero *et al.* 2018) as a proxy. The ingestion of these artificial molecules can occur in the absence of bacterial food (Kiyama *et al.* 2012; Rodríguez-Palero *et al.* 2018), which may be seen as a disadvantage or an advantage depending on the application. For example, if the research question requires measuring intake without the complication of bacterial multiplication and metabolism, then a proxy may be preferred.

The reduction in bioluminescence that results from naloxone treatment illustrates both a limitation and a possible advantage of using a signal from the ilux operon, which requires active bacterial metabolism. On the one hand, if the signal is completely abolished then measurement is impossible. On the other hand, knowing that a given treatment affects bacterial physiology may be useful information in interpreting any observed feeding differences, since drug effects on bacteria are known to also affect host physiology (Cabreiro *et al.* 2013; García-González *et al.* 2017; Scott *et al.* 2017a). As most *C. elegans* laboratories use *E. coli* OP50 as a food source, we also attempted to transform OP50 with the ilux plasmid, but were unsuccessful. It is likely that there are differences in worm behavior on OP50 and DH5α in some assays, as there are for other *E. coli* strains such as HB101 (Shtonda and Avery 2006); however, we found similar feeding rates between our DH5α-ilux and OP50-GFP experiments in this assay (compare Figure 2 to Figure S1, and compare Figure 3 to Figure S3). Another limitation of our method is its sensitivity: we were unable to detect single worm feeding, although this is likely to be possible using a higher magnification imaging system.

Wild *C. elegans* strains aggregate and feed in groups when grown in the laboratory, much like the *npr-1* mutants studied here, while the N2 laboratory reference strain consists of solitary feeders (de Bono and Bargmann 1998). The most commonly cited hypothesis to explain why wild isolates aggregate is that aggregation is useful to avoid high-oxygen environments that represent oxidative stress, UV damage, and desiccation risks (Rogers *et al.* 2006; Busch and Olofsson 2012). Based on our observations that DA609 worms clear bacteria inside clusters before moving onto new regions of the lawn (Figure 3, C and D), and that in larger swarms only the leading edge is in contact with bacteria (Figure 4, E and F), we speculate that collective feeding may also be a kind of hygienic behavior. Pathogenic bacteria can infect *C. elegans* through cuticle attachment (Hodgkin *et al.* 2000, 2013), and collective feeding may mitigate the risk of infections by reducing surface exposure to bacteria.

Acknowledgments

ilux pGEX(-) was a gift from Stefan Hell (Addgene plasmid #107879; http://n2t.net/addgene:107879; RRID: Addgene_107879). *E. coli* OP50-DsRed and OP50-GFP strains were gifts from Jonathan Hodgkin. Some worm strains were provided by the *Caenorhabditis* Genetics Center, which is funded by National Institutes of Health Office of Research Infrastructure Programs (P40 OD010440). We thank Alex Sardini for assisting with the IVIS Spectrum imaging system. This work was funded by the Biotechnology and Biological Sciences Research Council grant BB/N00065X/1 (to A.E.X.B.), by the European Union's Horizon 2020 programme under the Marie Skłodowska-Curie grant 842860 (to M.R.), and by the Medical Research Council through grants MC-A658-5TY30 (to A.E.X.B.) and MC-A658-5QEA0 (to K.S.S.). K.S.S. is supported by an Imperial College Research Fellowship.

Literature Cited

Andersen, E. C., J. S. Bloom, J. P. Gerke, and L. Kruglyak, 2014 A variant in the neuropeptide receptor npr-1 is a major determinant of Caenorhabditis elegans growth and physiology. PLoS Genet. 10: e1004156 (erratum: PLoS Genet. 10: e1004156). https://doi.org/10.1371/journal.pgen.1004156

Avery, L., 1993 The genetics of feeding in Caenorhabditis elegans. Genetics 133: 897–917.

Avery, L., and B. B. Shtonda, 2003 Food transport in the C. elegans pharynx. J. Exp. Biol. 206: 2441–2457. https://doi.org/10.1242/jeb.00433

Avery L., and Y.-J. You, 2012 *C. elegans* feeding (May 21, 2012), *WormBook*, ed. The *C. elegans* Research Community, WormBook, doi/10.1895/wormbook.1.150.1, http://www.wormbook.org.

Balasubramanian, P., P. R. Howell, and R. M. Anderson, 2017 Aging and caloric restriction research: a biological perspective with translational potential. EBioMedicine 21: 37–44. https://doi.org/10.1016/j.ebiom.2017.06.015

Bendesky, A., M. Tsunozaki, M. V. Rockman, L. Kruglyak, and C. I. Bargmann, 2011 Catecholamine receptor polymorphisms affect decision-making in C. elegans. Nature 472: 313–318. https://doi.org/10.1038/nature09821

Bernstein, R. A., 1975 Foraging strategies of ants in response to variable food density. Ecology 56: 213–219. https://doi.org/10.2307/1935314

Bhatla, N., R. Droste, S. R. Sando, A. Huang, and H. R. Horvitz, 2015 Distinct neural circuits control rhythm inhibition and spitting by the myogenic pharynx of C. elegans. Curr. Biol. 25: 2075–2089. https://doi.org/10.1016/j.cub.2015.06.052

Bokman, S. H., and W. W. Ward, 1981 Renaturation of Aequorea green-fluorescent protein. Biochem. Biophys. Res. Commun. 101: 1372–1380. https://doi.org/10.1016/0006-291X(81)91599-0

Brenner, S., 1974 The genetics of Caenorhabditis elegans. Genetics 77: 71–94.

Busch, K. E., and B. Olofsson, 2012 Should I stay or should I go? Worm 1: 182–186. https://doi.org/10.4161/worm.20464

Cabreiro, F., C. Au, K.-Y. Leung, N. Vergara-Irigaray, H. M. Cochemé *et al*., 2013 Metformin retards aging in C. elegans by altering microbial folate and methionine metabolism. Cell 153: 228–239. https://doi.org/10.1016/j.cell.2013.02.035

Cheong, M. C., A. B. Artyukhin, Y.-J. You, and L. Avery, 2015 An opioid-like system regulating feeding behavior in C. elegans. eLife 4: e06683. https://doi.org/10.7554/eLife.06683

Choi, S., M. Chatzigeorgiou, K. P. Taylor, W. R. Schafer, and J. M. Kaplan, 2013 Analysis of NPR-1 reveals a circuit mechanism for behavioral quiescence in C.elegans. Neuron 78: 869–880. https://doi.org/10.1016/j.neuron.2013.04.002

de Boer, H. A., L. J. Comstock, and M. Vasser, 1983 The tac promoter: a functional hybrid derived from the trp and lac promoters. Proc. Natl. Acad. Sci. USA 80: 21–25. https://doi.org/10.1073/pnas.80.1.21

de Bono, M., and C. I. Bargmann, 1998 Natural variation in a neuropeptide Y receptor homolog modifies social behavior and food response in C. elegans. Cell 94: 679–689. https://doi.org/10.1016/S0092-8674(00)81609-8

Demir E., Y. I. Yaman, and A. Kocabas, 2019 Dynamics of pattern formation and emergence of swarming in C. elegans. arXiv 1906.10067. https://arxiv.org/abs/1906.10067

Ding, S. S., L. J. Schumacher, A. E. Javer, R. G. Endres, and A. E. Brown, 2019a Shared behavioral mechanisms underlie C. elegans aggregation and swarming. eLife 8: e43318. https://doi.org/10.7554/eLife.43318

Ding, S. S., L. S. Muhle, A. E. X. Brown, L. J. Schumacher, and R. Endres, 2019b Comparison of solitary and collective foraging strategies of *Caenorhabditis elegans* in patchy food distributions. bioRxiv. https://doi.org/10.1101/744649

Djalalinia, S., M. Qorbani, N. Peykari, and R. Kelishadi, 2015 Health impacts of obesity. Pak. J. Med. Sci. 31: 239–242. https://doi.org/10.12669/pjms.311.7033

Fang-Yen, C., L. Avery, and A. D. T. Samuel, 2009 Two size-selective mechanisms specifically trap bacteria-sized food particles in Caenorhabditis elegans. Proc. Natl. Acad. Sci. USA 106: 20093–20096. https://doi.org/10.1073/pnas.0904036106

García-González, A. P., A. D. Ritter, S. Shrestha, E. C. Andersen, L. S. Yilmaz *et al*., 2017 Bacterial metabolism affects the C. elegans response to cancer chemotherapeutics. Cell 169: 431–441.e8. https://doi.org/10.1016/j.cell.2017.03.046

Gloria-Soria, A., and R. B. R. Azevedo, 2008 npr-1 regulates foraging and dispersal strategies in Caenorhabditis elegans. Curr. Biol. 18: 1694–1699. https://doi.org/10.1016/j.cub.2008.09.043

Gomez-Amaro, R. L., E. R. Valentine, M. Carretero, S. E. LeBoeuf, S. Rangaraju *et al*., 2015 Measuring food intake and nutrient absorption in *Caenorhabditis elegans*. Genetics 200: 443–454. https://doi.org/10.1534/genetics.115.175851

Gregor, C., K. C. Gwosch, S. J. Sahl, and S. W. Hell, 2018 Strongly enhanced bacterial bioluminescence with the ilux operon for single-cell imaging. Proc. Natl. Acad. Sci. USA 115: 962–967. https://doi.org/10.1073/pnas.1715946115

Harvey, S. C., 2009 Non-dauer larval dispersal in *Caenorhabditis elegans*. J. Exp. Zoolog. B Mol. Dev. Evol. 312B: 224–230. https://doi.org/10.1002/jez.b.21287

Hodgkin, J., P. E. Kuwabara, and B. Corneliussen, 2000 A novel bacterial pathogen, Microbacterium nematophilum, induces morphological change in the nematode C. elegans. Curr. Biol. 10: 1615–1618. https://doi.org/10.1016/S0960-9822(00)00867-8

Hodgkin, J., M.-A. Félix, L. C. Clark, D. Stroud, and M. J. Gravato-Nobre, 2013 Two leucobacter strains exert complementary virulence on Caenorhabditis including death by worm-star formation. Curr. Biol. 23: 2157–2161. https://doi.org/10.1016/j.cub.2013.08.060

Horvitz, H. R., M. Chalfie, C. Trent, J. E. Sulston, and P. D. Evans, 1982 Serotonin and octopamine in the nematode Caenorhabditis elegans. Science 216: 1012–1014. https://doi.org/10.1126/science.6805073

Kiyama, Y., K. Miyahara, and Y. Ohshima, 2012 Active uptake of artificial particles in the nematode Caenorhabditis elegans. J. Exp. Biol. 215: 1178–1183. https://doi.org/10.1242/jeb.067199

Lanan, M., 2014 Spatiotemporal resource distribution and foraging strategies of ants (Hymenoptera: formicidae). Myrmecol. News Osterreichische Ges. Entomofaunist. 20: 53–70.

Larsen, C. S., 2003 Animal source foods and human health during evolution. J. Nutr. 133: 3893S–3897S. https://doi.org/10.1093/jn/133.11.3893S

Lockery, S. R., S. E. Hulme, W. M. Roberts, K. J. Robinson, A. Laromaine *et al*., 2012 A microfluidic device for whole-animal drug screening using electrophysiological measures in the nematode C. elegans. Lab Chip 12: 2211–2220. https://doi.org/10.1039/c2lc00001f

MacArthur, R. H., and E. R. Pianka, 1966 On optimal use of a patchy environment. Am. Nat. 100: 603–609. https://doi.org/10.1086/282454

Maier, L., M. Pruteanu, M. Kuhn, G. Zeller, A. Telzerow *et al*., 2018 Extensive impact of non-antibiotic drugs on human gut bacteria. Nature 555: 623–628. https://doi.org/10.1038/nature25979

Mattson, M. P., D. B. Allison, L. Fontana, M. Harvie, V. D. Longo *et al*., 2014 Meal frequency and timing in health and disease. Proc. Natl. Acad. Sci. USA 111: 16647–16653. https://doi.org/10.1073/pnas.1413965111

McKay, J. P., D. M. Raizen, A. Gottschalk, W. R. Schafer, and L. Avery, 2004 eat-2 and eat-18 are required for nicotinic neurotransmission in the Caenorhabditis elegans pharynx. Genetics 166: 161–169. https://doi.org/10.1534/genetics.166.1.161

Milward, K., K. E. Busch, R. J. Murphy, M. de Bono, and B. Olofsson, 2011 Neuronal and molecular substrates for optimal foraging in Caenorhabditis elegans. Proc. Natl. Acad. Sci. USA 108: 20672–20677. https://doi.org/10.1073/pnas.1106134109

Niacaris, T., and L. Avery, 2003 Serotonin regulates repolarization of the C. elegans pharyngeal muscle. J. Exp. Biol. 206: 223–231. https://doi.org/10.1242/jeb.00101

Nicholls, S. B., and J. A. Hardy, 2013 Structural basis of fluorescence quenching in caspase activatable-GFP. Protein Sci. 22: 247–257. https://doi.org/10.1002/pro.2188

Pratt V., 1987 Direct least-squares Fitting of algebraic surfaces. ACM Comput. Graphics (Siggraph) 21: 145–152. https://doi.org/10.1145/37401.37420

Raizen, D. M., R. Y. Lee, and L. Avery, 1995 Interacting genes required for pharyngeal excitation by motor neuron MC in Caenorhabditis elegans. Genetics 141: 1365–1382.

Rodríguez-Palero, M. J., A. López-Díaz, R. Marsac, J.-E. Gomes, M. Olmedo *et al.*, 2018 An automated method for the analysis of food intake behaviour in Caenorhabditis elegans. Sci. Rep. 8: 3633. https://doi.org/10.1038/s41598-018-21964-z

Rogers, C., A. Persson, B. Cheung, and M. de Bono, 2006 Behavioral motifs and neural pathways coordinating O2 responses and aggregation in C. elegans. Curr. Biol. 16: 649–659. https://doi.org/10.1016/j.cub.2006.03.023

Sawin, E. R., R. Ranganathan, and H. R. Horvitz, 2000 C. elegans locomotory rate is modulated by the environment through a dopaminergic pathway and by experience through a serotonergic pathway. Neuron 26: 619–631. https://doi.org/10.1016/S0896-6273(00)81199-X

Scholz, M., D. J. Lynch, K. S. Lee, E. Levine, and D. Biron, 2016 A scalable method for automatically measuring pharyngeal pumping in C. elegans. J. Neurosci. Methods 274: 172–178. https://doi.org/10.1016/j.jneumeth.2016.07.016

Scott, T. A., L. M. Quintaneiro, P. Norvaisas, P. P. Lui, M. P. Wilson *et al.*, 2017a Host-microbe Co-metabolism dictates cancer drug efficacy in C. elegans. Cell 169: 442–456.e18. https://doi.org/10.1016/j.cell.2017.03.040

Scott, E., A. Hudson, E. Feist, F. Calahorro, J. Dillon *et al.*, 2017b An oxytocin-dependent social interaction between larvae and adult C. elegans. Sci. Rep. 7: 10122. https://doi.org/10.1038/s41598-017-09350-7

Shtonda, B. B., and L. Avery, 2006 Dietary choice behavior in Caenorhabditis elegans. J. Exp. Biol. 209: 89–102. https://doi.org/10.1242/jeb.01955

Stenberg, M., and A. Persson, 2005 The effects of spatial food distribution and group size on foraging behaviour in a benthic fish. Behav. Processes 70: 41–50. https://doi.org/10.1016/j.beproc.2005.04.003

Trepanowski, J. F., R. E. Canale, K. E. Marshall, M. M. Kabir, and R. J. Bloomer, 2011 Impact of caloric and dietary restriction regimens on markers of health and longevity in humans and animals: a summary of available findings. Nutr. J. 10: 107. https://doi.org/10.1186/1475-2891-10-107

You, Y., J. Kim, D. M. Raizen, and L. Avery, 2008 Insulin, cGMP, and TGF-β signals regulate food intake and quiescence in C. elegans: a model for satiety. Cell Metab. 7: 249–257. https://doi.org/10.1016/j.cmet.2008.01.005

Zhao, Y., L. Long, W. Xu, R. F. Campbell, E. E. Large *et al.*, 2018 Changes to social feeding behaviors are not sufficient for fitness gains of the Caenorhabditis elegans N2 reference strain. eLife 7: e38675. https://doi.org/10.7554/eLife.38675

Communicating editor: H. Buelow